International Journal of Industrial Electronics, Control and Optimization © 2020 IECO
Vol. 3, No. 2, pp. 173-186, April (2020)

# Introducing a New Hybrid Adaptive Local Optimal Low Rank Approximation Method for Denoising Images

Sadegh Kalantari [1,†], Mehdi Ramezani [2], and Ali Madadi [3]

[1,2,3] Department of Electrical Engineering, University of Tafresh, Tafresh, Iran

**ABSTRACT**

*This paper aimed to formulate image noise reduction as an optimization problem and denoise the target image using matrix low rank approximation. Considering the fact that the smaller pieces of an image are more similar (more dependent) in natural images; therefore, it is more logical to use low rank approximation on smaller pieces of the image. In the proposed method, the image corrupted with AWGN (Additive White Gaussian Noise) is locally denoised, and the optimization problem of low rank approximation is solved on all fixed-size patches (Windows with pixels needing to be processed). For practical purposes, this method can be implemented parallelly, because it can simultaneously handle different image patches. This is one of the advantages of this method. In all noise reduction methods, the two factors, namely the amount of the noise removed from the image and the preservation of the edges (vital details), are very important. In the proposed method, all the new ideas -including the use of TI image (Training Image) and SVD adaptive basis, iterability of the algorithm and patch labeling- have all been proved efficient in producing sharper images, and good edge preservation. They also had an acceptable speed compared to the state-of-the-art denoising methods.*

**Article Info**

***Keywords:***
Optimal Low Rank Approximation, SVD, Signal Denoising, Image Denoising, Signal Processing, Optimization

***Article History:***
**Received** 2019-08-08
**Accepted** 2019-12-13

## I. INTRODUCTION

Signal denoising is one of the most important issues in the field of digital image processing. Noise might destroy or damage vital information and details of a signal. Therefore, denoising is one of the initial stages of the process of features extraction, object recognition, image matching, and etc. Several methods have been proposed to denoise digital images and signals unitl now [1-11].

AWGN is one of the most significant noises studied by researchers. In each pixel of the noisy image built by AWGN, a value is added to its gray level. This value is sampled independently from Gaussinan distribution.

AWGN denoising methods can be divided into three categories including correlation-based (or spatial filter), transform-based and hybrid methods. Correlation-based methods work directly with spatial values of the image. The advantages of correlation-based methods include simplicity of its algorithms and their acceptable speed. In transform-based methods, the image is first transferred to the desired transform domain and then denoised. Therefore, applying transformation to a signal is equivalent to changing the axes of the coordinates. Changing the coordinates of the signal makes it possible to effectively separate the noisy and non-noisy part of the signal which itself is one of the advantages of these methods. The hybrid methods take advantage of both these methods simultaneously.

In the process of image denoising, the amount of eliminated noise as well as the preserved edge and textures are

† Corresponding Author: Sadeghkalantari@tafreshu.ac.ir
Tel: +98-8636241261, Faculty of Electrical Engineering, University of Tafresh, Tafresh, Iran

considered as the most important issues. Moving Average and Gaussian Filter are regared as the easiest correlation-based methods. These methods like a low pass filter soften the high-frequency parts of the image (including noise and edges). Despite their good denoising capability, the mentioned methods eliminate some of the tiny yet vital information. BF (Bilateral Filter) has been used to improve edge preservation [11]. In this filter, the value of each pixel is estimated by the average weight of the neighbors. Intensity and spatial similarity was the criterion by which the weight of the neighbors was determined. This preserves sharp edges during denoising; however, the staircase effect and gradient reversal are the disadvantages of this method. NLM method is a non-local version of BF which estimates the value of each pixel using the weighted average of the similar pixels. In this method, the weights are determined based on the similarity between the pixels. Simplicity of the algorithm and relatively convenient speed are among the advantages of this method.

In transform-based methods, the images can be represented using some sparse bases like Wavelet, Curvelet and Contourlet [12]. Some of these bases are fixed, but some are selected adaptively and adapted to the signal information. Because of complex singularities in many images, using fixed basis such as wavelet will not always yield acceptable results. Two methods [13] and [14] have proposed an adaptive representation method called K-SVD. In these methods, an optimization problem is solved using greedy algorithms. Then, a dictionary is trained in order to denoise the image. The columns (atoms) of this dictionary can be used as an adaptive basis for sparse representation. Today, the use of sparse representation in many applications such as denoising, super-resolution, image reconstruction, inpainting, and etc has provided acceptable results [15-17]. Noise spreads over all transform coefficients. However, most of the basic image information is focused only on a few of the largest coefficients. Hence, in such methods image denoising can be done using many shrinkage methods such as [18]. In general, methods such as K-SVD, [19] and [20] which solve an optimization problem in order to denoise an image are called optimization-based methods. These methods are considered as transform-based methods. Since these methods solve optimization problems, they usually have a lot of computational complexity and are slow.

The BM3D is one of the hybrid methods in which spatial filtering and transform-based methods are used [21]. This method denoises the image by sparse filtering and grouping similar patches into 3d arrays. Two-dimensional patches are a window of the image that is extracted by overlapping. In general, the overlap value is different, but for the maximum overlap the step length is one pixel. Today, more complete versions of BM3D method have been presented. These new methods have improved the results using shape-adaptive principal component analysis [22]. Some of the hybrid methods like ASVD and SAIST take advantage of useful properties of SVD basis. ASVD method uses SVD for training basis in order to represent the image patches. SAIST method denoises image using SVD and sparse representation of image patches [23, 24]. The unique feature of these methods is that they combine the most useful properties of both correlation-based and transform-based methods; therefore, the output images provide better results in terms of speed and quality.

This paper intends to provide an adaptive local denoising method using adaptive SVD basis. In this method, a TI (Training Image) is created using noisy image and Gaussian filter. The resulted TI is used in signal denoising. Based on the locality of the algorithm, SVD is computed for all image patches (with maximum overlapping i.e. one pixel step length) and then each patch is denoised individually and adaptively using TI information. In order to prevent artifacts, aggregation phase is done after computing estimated patches. In this phase, the average obtained values are replaced in overlapping areas. Since these methods can consider each patch both individually and in parallel with other patches, they can be implemented for practical purposes. Considering the ideas in the proposed method, it belongs to the family of hybrid methods.

In this study, using the above-mentioed ideas, a denoising method having appropriate quantitative factors (PSNR and FSIM) and acceptable computational complexity is proposed. In addition to its sharp and high quality images, another benefit of this method is that it solves the noise problem and increases the efficiency by combining some of the common image processing methods and using the information of the noisy image.

Various sections of the article are as follows. In section 2, the linear representation of the image was examined using SVD and low rank approximation problem was formulated. In sections 3 and 4, the proposed method was presented and the applied ideas were explained. In sections 5 and 6, the results of the proposed method and the conclusions were presented respectively.

## II. SVD AND LOW RANK APPROXIMATION

Suppose $A$ represents a gray level image. The basic principle of linear representation of the image is that matrix $A$ can be represented as the sum of the weighted basis shown in (1). In this equation, $a_i$ are the coefficiants and $\phi_i$ are the corresponding bases. These bases can be chosen from well-known bases like wavelet, curvelet, bandlet, contourlet and etc [25-28].

$$A = \sum_{i=1}^{N} a_i \phi_i \tag{1}$$

These bases are similar to the Fourier series. Each periodic 2d

function can be represented in terms of exponential basis and $C_{mn}$ coefficients are according to Equ. (2).

$$f(x,y)=\sum_{n=-\infty}^{+\infty}\sum_{m=-\infty}^{+\infty}C_{mn}e^{\frac{im\pi x}{a}}.e^{\frac{im\pi y}{b}},-a<x<a,$$
$$-b<y<b,C_{mn}=\frac{1}{ab}\int_{-a}^{a}\int_{-b}^{b}f(x,y)e^{\frac{-in\pi x}{a}}.e^{\frac{-im\pi y}{b}}dxdy \quad (2)$$

According to the expansion of the Riemann–Lebesgue lemma, $C_{mn}$ coefficients are descending and the result will be as Equ. (3) [29].

$$\lim_{m\to\infty}\lim_{n\to\infty}C_{mn}=0 \quad (3)$$

This lemma states that the high harmonic coefficients are negligible and they have very little effect on reconstructing the signal. So, if the coefficients are truncated from a specified frequency onward, the original signal can be reconstructed with a fairly good approximation. In the next section, the idea of truncation is used for denoising the signal with SVD. In SVD theory, each matrix can be decomposed as Equ. (4).

$$A=U\Sigma V^t \quad (4)$$

In which $U_{m\times m}=[u_1...u_m]$ (left singular vector) and $V_{n\times n}=[v_1...v_n]$ (right singular vector) are orthogonal matrix. So according to Equ. (5):

$$VV^t=V^tV=I_n,$$
$$UU^t=U^tU=I_m. \quad (5)$$

It should be noted that the columns of $U_{m\times m}$ and $V_{n\times n}$ matrices are composed of $AA^t$ and $A^tA$ orthonormal eigenvectors matrices respectively. $\Sigma_{m\times n}$ is a semi-diagonal matrix in which the values on its diagonal are the singular values of the $A^tA$ or $AA^t$ matrices. So we will have:

$$\Sigma_{m\times n}=diag(\sigma_1,...,\sigma_p),p=\min\{m,n\}$$
$$\sigma_1\geq\sigma_2\geq...\geq\sigma_k>0,\sigma_{k+1}=...=\sigma_p=0 \quad (6)$$

in which $\sigma_1$ is the largest and $\sigma_k$ is the smallest non-zero singular value of matrix $A$.

### A. *Formulation of Low Rank Approximation Problem*

Approximation of a matrix with a lower rank one can be done using SVD. The goal in this section is to estimate low rank matrix $B$ using matrix $A$. According to Equ. (7), in singular value decomposition of matrix $A$ with rank $r$, we will have:

$$A=[U_1\,|\,U_2]\begin{bmatrix}\sigma_1&0&0&\\0&\ddots&0&0\\0&0&\sigma_r&\\&0&&0\end{bmatrix}\begin{bmatrix}V_1^T\\\hline V_2^T\end{bmatrix},\quad rank(A)=r. \quad (7)$$

According to definition of the two matrices $U$ and $V$, the singular value decomposition of matrix $A$ can be represented as shown in Equ. (8):

$$A=u_1\sigma_1v_1^t+u_2\sigma_2v_2^t+...+u_r\sigma_rv_r^t,\ \sigma_1>\sigma_2>...>\sigma_r. \quad (8)$$

In general, we represent matrix $A$ linearly in the form of (9) or (10) equations according to SVD of $A$.

$$A=[U_{1a}\,|\,U_{1b}\,|\,U_2]\begin{bmatrix}\sigma_1&&0&&&&\\&\ddots&&&0&&0\\0&&\sigma_k&&&&\\&&&\sigma_{k+1}&&0&\\&0&&&\ddots&&0\\&&&0&&\sigma_{r+1}&\\&0&&&0&&0\\&&&&&&\end{bmatrix}\begin{bmatrix}V_{1a}^T\\\hline V_{1b}^T\\\hline V_2^T\end{bmatrix} \quad (9)$$

$$A=u_1\sigma_1v_1^t+...+u_k\sigma_kv_k^t+u_{k+1}\sigma_{k+1}v_{k+1}^t+...+u_r\sigma_rv_r^t$$
$$=\sigma_1u_1v_1^t+...+\sigma_ku_kv_k^t+\sigma_{k+1}u_{k+1}v_{k+1}^t+...+\sigma_ru_rv_r^t \quad (10)$$
$$A=\sum_{i=1}^{r}a_i\phi_i$$

Comparing Equ. (1) and Equ. (10), we can see that $\sigma_i$ are coefficients and $u_iv_i$ the corresponding bases, which unlike the constant bases of Fourier series, are selected adaptively using signal information. According to Equ. (11):

$$\sigma_1>\sigma_2>...>\sigma_r \quad . \quad (11)$$

Primary coefficients play a greater role in reconstructing matrix $A$. This also applies to representing a signal by the Fourier Series baesd on Riemann–Lebesgue lemma.

Now the main problem is to determine $B$ (the low rank approximation of the matrix $A$) as an optimization problem in the form of (12):

$$B=\arg\min_z\ \|A-z\|_2^2\quad st.\quad rank(z)=k. \quad (12)$$

In the above statement, $k$ is regarded as 'sparsity'. Assuming applying SVD on matrix $A$, and considering Eckart-Young-Mirsky's theorem which is available in [30], and also Equ. (9), the closed form answer for the optimization problem in (13) is as follows:

$$\Sigma_B = diag(\sigma_1, \sigma_2, ..., \sigma_k, 0, 0, ...0)$$
$$B = U\Sigma_B V^t = u_1\sigma_1 v_1^t + u_2\sigma_2 v_2^t + ... + u_k\sigma_k v_k^t \Rightarrow$$
$$B = U_{1a}\begin{bmatrix}\sigma_1 & & 0\\ & \ddots & \\ 0 & & \sigma_k\end{bmatrix}V_{1a}^t = U_{1a}\Sigma_B V_{1a}^t \quad . \tag{13}$$

The theorem in the above reference describes a criterion for calculating the optimal value of $k$ as (14):

$$\sum_{i=1}^{k}\sigma_i^2 \geq \sum_{i=K+1}^{p}\sigma_i^2 \quad , \quad p = \min\{m,n\} \quad . \tag{14}$$

In accordance with the above criterion, the sum of the $k$ values of retained singular values must be greater than (or equal to) the sum of the truncated values so that an appropriately low rank approximation of $A$ can be obtained. Now, considering the discussions in the next section, we will discuss how to eliminate noise using SVD.

### *B. Signal Denoising in one-dimensional noisy signals using SVD*

Signal denoising is one of the applications of low rank approximation. Assume that we have sampled the continuous time signal $x(t)$ and represented $x = [x_1\ x_2\ x_3 ... x_{m\times n}]$ as a vector. Now we can classify the samples in an appropriate order and represent them as matrix $A$.

$$A_{m\times n} = \begin{bmatrix} x_1 & x_{m+1} & x_{2m+1} & \cdots \\ x_2 & x_{m+2} & x_{2m+2} & \cdots \\ \vdots & \vdots & \vdots & \vdots \\ x_m & x_{2m} & x_{3m} & \cdots \end{bmatrix}$$

According to Equ. (15), if we compute the singular values of matrix $A$, some of them will be much larger than the other singular values, and smaller coefficients will have fewer roles in creating the matrix structure [12].

$$A = \sigma_1 u_1 v_1^t + \sigma_2 u_2 v_2^t + ... + \sigma_k u_k v_k^t + \sigma_{k+1} u_{k+1} v_{k+1}^t + ... + \sigma_r u_r v_r^t \tag{15}$$

Now consider the following noisy signal:

$$x_n = x + n \tag{16}$$

In the above equation, $x_n$ is a noisy signal, $x$ is the noise-free signal and $n$ is noise. Noise increases the significance of the last sentences by increasing the smaller singular values of the matrix (or signal), thereby destroying the original structure of the matrix. If these sentences can be truncated (or at least their impact in reconstructing the signal is minimized), signal denoising will be possible using low rank approximation. In order to test the denoising method using Eckart-Young-Mirsky criteria, two one-dimensional noisy signals are denoised and the results are shown in Fig.1. It should be noted that the number of samples in these tests was 100 and they were arranged in a $10\times 10$ matrix. In the following tests, $k$ is sparsity of the semidiagonal matrix $\Sigma$ that is determined using Eckart-Young-Mirsky criterion. For example, $k=3$ means the signal is reconstructed (denoised) by 3 of the largest singular values. The following results show that truncation of smaller singular values has improved the noisy signals.

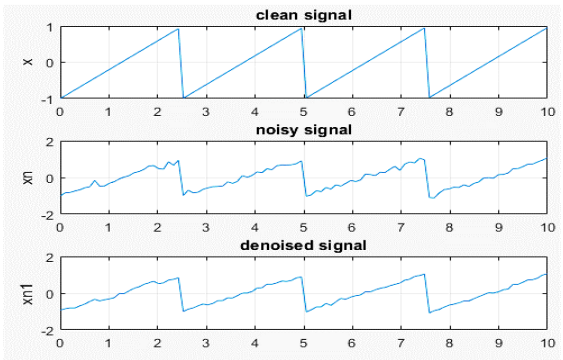


a) $k=3$

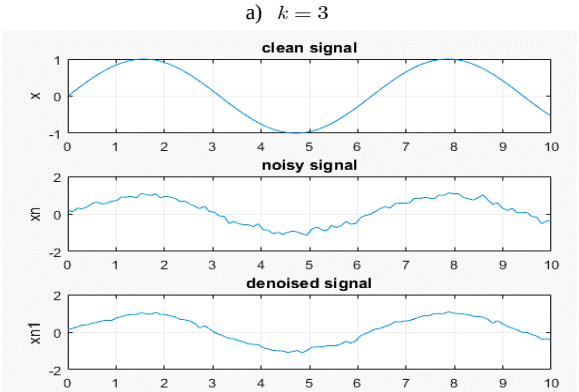


b) $k=2$

**Fig. 1.** The results of applying noise reduction method on two noisy signals using SVD and Eckart-Young-Mirsky criteria

## III. PRODUCTION OF TI IMAGE

Due to the fact that noise appears at high frequencies, image denoising using Gaussian filter is one of the easiest ways. High-frequency parts of the image (edges + details) and noise are somewhat destroyed after applying the Gaussian filter to the image. In other words, the resulted image is smoothed (blurred). Using this filter, we can decompose the high and low frequency components of the image. In general, each image can be decomposed into sum of a low-frequency (general details) and a high-frequency image (including edges and fine details). For example, Fig.2 shows the decomposition of a noisy image into two high frequency and low frequency images, respectively. After separating the high frequency and the low frequency components, we could separate the noise+edge image from the noisy one (the high frequency component of the image). Then, the noise+edge image was denoised using low frequency component. Finally, a denoised image was generated by integrating the denoised

high frequency and the low frequency components. Using this idea, we can use the information contained in the image itself, and obtain a higher accuracy in the process of truncating the SVD coefficients.

Based on the analysis, the larger SVD coefficients (low-frequency ones) contain the coarse details of the image, and smaller coefficients (high frequency ones) include fine details and noise. Therefore, in case the coefficients can be truncated adaptively using low frequency component information, the output denoised image will have an acceptable sharpness as well.

As it is clear, if a noisy signal is derived for the edge detection (structures and textures which have sudden changes), the result will be noisy. So, the derivation of the resulting signal will not useful for identifying the edges. In order to prevent this problem, the signal must be smoothed. That is, it must be passed through a low pass filter (Gaussian filter) so that the high-frequency components become less effective. Then, it can be derived to reveal the edges. Given the AWGN noise and the definition of the standard deviation calculation, in this paper, the standard deviation of the Gaussian filter for each image is estimated using Equ. (17). For matrix or image $A_{m\times n}$, $a_{ij}$ refers to the elements of $A$ and $\mu_A$ is it's average.

$$\sigma = \frac{\sum_{i=1}^{m}\sum_{j=1}^{n}(a_{ij}-\mu_A)^2}{m\times n}, \qquad \mu_A = 0. \tag{17}$$

For the reasons given, to identify the edges and structured areas in the image, first we pass the image from a low pass filter to minimize the effects of noise, then it is derived (canny algorithm) and the edges of the image are found. Fig. 3 shows these steps. As we can see from the above figures, we were able to detect the critical edges of the image (Training Image) with an acceptable accuracy using the idea of filtering the image with Gaussian filters and extracting the edge using the low-frequency component. The training image information was used to remove noise from the noise + edge image. After denoising the noise+edge image, it will be combined with the low-frequency component and a denoised image will be created.

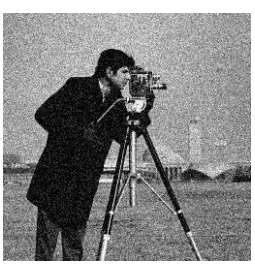

Original Noisy Image

Low frequency Noisy Image (standard deviation = 4)

High Frequency Image (High Frequency Component)

**Fig. 2**. Decomposing low frequency and high frequency components of Noisy image using Gaussian filter

Noisy Image

Low frequency component of noisy image with w=15 and standard deviation=6.

Extracted edges using canny method

Noise + Image edges

**Fig. 3**. Production of TI and Noise+Edges image from a noisy image

## IV. THE PROPOSED METHOD

In the previous section, we were able to determine the image edge (important parts of the image structures) using a Gaussian filter from the noisy image. The result can be used as a training image, or as a model for detection of texured areas. The resulting TI makes it possible to use the information in the noisy image to eliminate the noise adaptively. According to the results gained from Fig. 4, some noise reduction methods like [20] eliminate many critical details and blur the output image. In this section, based on the reviewed basics and ideas, a new algorithm is proposed which, in addition to eliminating noise in smooth areas, improves the output image sharpness. The proposed method is shown in table I and Fig. 5.

As described before, we aimed to apply low-rank

approximation to smaller pieces of the image. Since the smaller parts in a natural image are more similar to each other, low rank approximation of smaller pieces is more justifiable. To do so, the singular value decomposition is calculated for each piece extracted from the image (the high frequency component of the noisy image). In order to better preserve the edges, the corresponding patches in the TI image were used. The pieces of the noisy image having low edges (the part of the image which is almost smooth) must be reconstructed with smaller singular values. The parts with more details must also be made with a greater number of singular values. Therefore, the corresponding patch in the TI image is also extracted for each patch of the noisy image in the proposed algorithm. If the average gradient in each patch exceeds the mean gradient of the total TI image, it indicates that the patch belongs to the textured parts of the image. So we use the ECKERT method to determine $k$. If the average gradient of the patch is less than the mean gradient of the total TI image, it indicates that the patch belongs to the smooth areas of the image. Therefore, in order to reduce the computational complexity, the $k$ value is considered to be 1. In addition to reducing the computational complexity, this idea preserves important and vital information in structured areas and prevents bluring. This operation is performed on all the extracted overlapping patches of the noisy image and the denoised image is created eventually. The patches are extracted from the image as a raster path with a maximum overlap (with one pixel in each step). Since there is an overlap between patches, multiple estimates can be obtained for different parts of the image. In those parts, the mean of those values is applied. This is called aggregation phase. For example, if two different values are obtained for a pixel (due to the overlap of windows), their average is considered as the final pixel value.

Since an optimization problem is solved in the noise reduction process, the proposed method can be considered as an optimization-based combination method. In order to reduce the computational complexity and increase the speed of the proposed algorithm, the patches of the image are labeled in terms of their similarity (patch labeling process). Therefore, in the preprocessing stage, before entering the low rank approximation process, the similarity of different patches of the TI image is examined using Euclidean distance, and the patches that are similar to each other carry the same label. Using Equ. (18), we can examine the similarity of two patches.

$$s(p_i, p_c) = \left\| p_i - p_c \right\|_2^2 \tag{18}$$

In the above equation, $\| \|_2$ refers to Euclidean distance; $p_i$ refers to vectorized reference patch; and $p_c$ refers to vectorized candidate patch. The smaller the value of $s(p_i, p_c)$, the more similar the two patches. The reference patch with $n$ number of the same patches together make up a group all patches of which have the same label. The computational complexity of the proposed method is reduced by labeling different TI patches and using the above idea. For all patches of a given group, $k$ value is considerd to be the same. In fact, $k$ value is only calculated for the agent of each group; the same value is considered for the rest of the patches of the same group.

Iterabilty of the algorithm is another idea which can improve the image quality. The output image is refined and the noise effects will be minimized by performing the above steps on the noisy image (in the first iteration) and the denoised image (in the next iteration). It should be noted this idea will increase the quality of the output image only for a limited number of iterations.

In summary, the important highlights of the proposed method are as follows:

- In this study, local optimal low rank approximation was done using Eckart-Young-Mirsky's theorem. The reason is that such theorm can solve the problem of low-rank approximation on small patches.
- For adaptive detection of textured areas, the training image was used in order to determine the sparsity and achieve sharp denoised images.
- Patch labeling was used to increase speed and accuracy.
- Adaptive SVD basis was used for representing and denoising the Image. This allows the noise removal process to be performed according to the information in the training image.
- The algorithm used in the study was quite simple because of the use of simple signal processing operations.
- This method can be implemented parallelly for practical purposes, because it can simultaneously handle different image patches.

**Fig. 4**. The result of method [20]

Table I. The proposed method

Input: Noisy Image $A$

Output: Denoised Image $H$

Parameters:: Patch Size, $n$ : The Number of Groups in Patch labeling, $iternum$ : The number of Iteration.

**Algorithm:**

Set $ws$ and $n$.

For $iter = 1$ to $iternum$ do

1-Decompose $A$ for first iteration and $H$ for other iteration to $A_L$ (Low Frequency Component) and $A_H$ (High Frequency Component) Using Part III.

2- Get the TI Image Using CANNY Edge detection and $A_L$ .

3- Do Patch Labeling on the TI with $n$ Group Using Part III.

4-For all of the Patches with $ws$ size in $A_H$ , Extract the Corresponding Patch in the TI Image. For Patches with the same label, set the value of $k$ equal to specified value fo their agent and go to step 6 .

5-If the Mean Gradient of the Patch is greater than the average gradient of the image, set $k$ with ECKERT Method, Otherwise set $k$ equal to 1.

6-Reconstruct the Patch with specified $k$ and Place it in the Corresponding Location in Denoised Image $H_H$ .

7-Do Aggregation phase.

8-Compute Denoised Image with following equation : $H = H_H + A_L$

## V. The Results of Proposed Method

In this section, the results of the proposed method are compared with the other methods including [19], [20], [3], [12] and [21]. [3], [19] and [20] are among the optimization-based methods and [12] and [21] are among the hybrid ones. The denoising problem is formulated in an optimization framework using kernel regression in [6], using joint statistical modeling in method [19] and using sparse representation in [20]. These methods are usually slow due to the difficulty of some optimization problems. Method [12] is similar to the proposed method in using SVD; and we expect its results to be close to those of the proposed method. Method [21] is expected to have good results in terms of PSNR and FSIM. Its low speed is due to the use of the sparse filtering of the patches and three-dimensional patch grouping.

The above methods were implemented on the standard test images of CAMERAMAN, LENA, PEPPERS, MANDRILL, BOATS, BARBARA, BRIDGE, PARROT, CAP, HOUSE and the performance of each method was investigated. The reason for using these standard images is their variability in texture and detail. Most aricles in this field actually evaluate the effectiveness of the proposed method on these images. Implementation of all algorithms are done using a computer with an Intel Corei7, 1.8GH processor, 6GB of RAM and with MATLAB software run under the Windows 8.1 operating system. In all experiments, the size of the CAMERAMAN image is 256 × 256, the size of the rest of Images is 512 × 512, and the noisy image is obtained by adding AWGN with various $\sigma_n$ to test images. To test the performance of the proposed method, PSNR (Peak Signal-to-Noise Ratio) and FSIM (Feature Similarity Index) criteria have been used. These two criteria are fully explained in the reference method [12]. Although PSNR criterion is calculated in all denoising methods, the quantity obtained does not correspond to human visual perception in some cases. Therefore, in addition to the PSNR, another measure called FSIM is also used. This criterion is obtained by measuring the similarity between the two images and combining the phase correlation property and the gradient magnitude. The higher the value of FSIM, the higher the quality of the images will be.

Appropriate parameters are selected by trial and error using numerical experiments. For proper selection of algorithm parameters like $n$, number of iterations, and patch size, the proposed method has been tested on the CAMERAMAN image and its results are reported in Table II. According to the results of Table II and Fig. 6, the following values are considered for the proposed method: $ws = 25$, $n = 1000$ and $iternum = 3$. The results of the proposed method as well as those of other methods are presented in Table III and Fig. 7. As indicated in the tests, the parameters selected in the other images in terms of PSNR, IEF and complexity of algorithm also have acceptable results. In this paper, for simple setting of parameters, they are considered equal for different images. For this reason, in some tests, the performance of the other methods has been better than the proposed method. However, the average of all tests shows the superiority of the proposed method over the other methods. However, the tests show that for more detailed images such as

Mandrill, it is better to have smaller groups and smaller patch sizes. For less detailed images, we need larger groups and larger window sizes.

The results of the proposed method are presented globaly and with various sparsities in Fig. 8. The effectiveness of the ideas like locality and an adaptive optimal $k$ in the proposed method can be investigated using Fig. 8. It is clear that the above ideas have improved the algorithm in terms of visual and PSNR criteria. Also, the results obtained using the above ideas are significantly superior to the other comparisons in terms of visual quality (sharpness of image and denoising) and PSNR criteria.

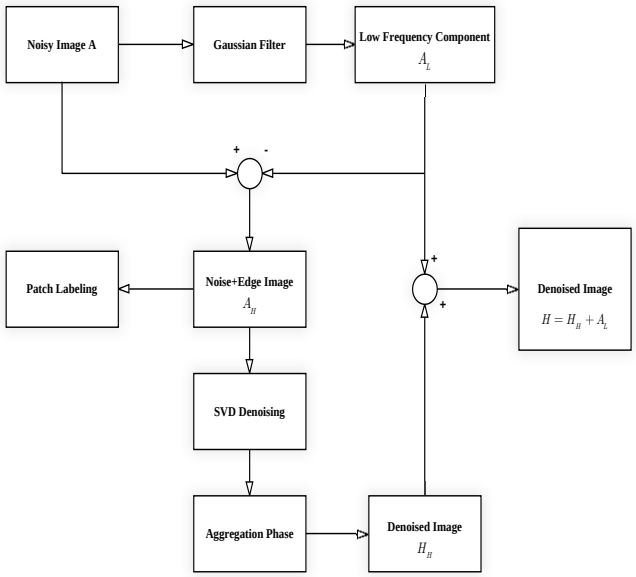


**Fig. 5** .Block Diagram of the Proposed Denoising Algorithm

To test the speed, different methods are compared in terms of runtime in the same conditions and the results are presented in Table IV. As expected, the reference methods [3], [19] and [20] are slower than the proposed method because they are among optimization-based methods. The runtime of method [12] is closer to that of the proposed method; and that is because of its similarity to the proposed method. Method [21] is also slower than the proposed method. That is due to the technique used to group similar patches into three-dimensional arrays.

Also, according to the results obtained in this section, the results of the proposed method is comparable and even superior to the state-of-the-art denoising methods in terms of PSNR, FSIM and edge preservation. This is due to the fact that the TI obtained from the noisy image has been used to determine optimal $k$ . It is noteworthy that $k$ helps to maintain useful details in the textured parts of the image. Since the proposed method is considered as one of the optimization-based hybrid methods, it is expected that the execution time of the algorithm will take longer than the other methods. However, the computational complexity of the proposed method has been greatly reduced, and the speed of the proposed algorithm is acceptable compared to the other methods; and that is because of patch labeling and using the same sparsity for similar patches. Finally, the proposed method was able to provide an acceptable performance in terms of quantitative and visual evaluation as well as algorithm speed; and it was because of implementing the ideas related to local adaptive SVD basis, using the training image, employing patch labeling and the repeatability of the method.

**Table II.** Sensitivity Analysis of the proposed method parameters on the CAMERAMAN image with $\sigma_n = 10$

| n | Patch Size ( $ws$ ) | PSNR(dB) |
|---|---|---|
| 500 | 9 | 34.17 |
| 500 | 17 | 34.32 |
| 500 | 25 | 34.22 |
| 500 | 35 | 34.07 |
| 1000 | 9 | **34.37** |
| 1000 | 17 | **34.44** |
| 1000 | 25 | **34.54** |
| 1000 | 35 | **34.28** |
| 2000 | 9 | 34.2 |
| 2000 | 17 | 34.31 |
| 2000 | 25 | 34.15 |
| 2000 | 35 | 34.11 |
| 3000 | 9 | 34.11 |
| 3000 | 17 | 34.12 |
| 3000 | 25 | 34.04 |
| 3000 | 35 | 34.01 |

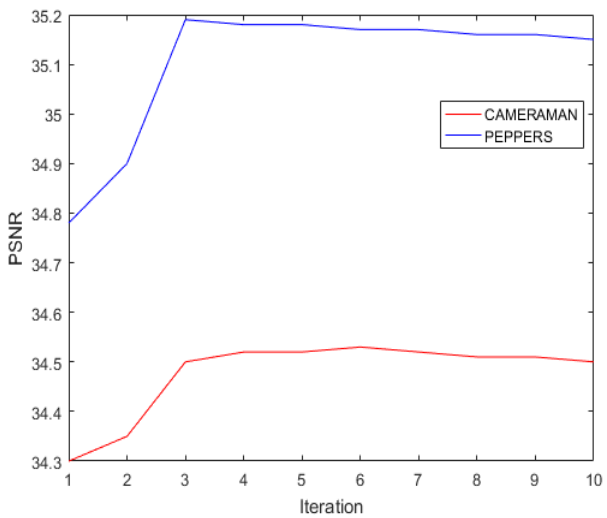


**Fig.6**. Effects of the number of iterations on the CAMERAMAN and PEPPERS Images.

**Table III**. The results of different methods on standard test images

| Image | $\sigma_n$ (Noise Level) | Method [19] PSNR | Method [19] FSIM | Method [20] PSNR | Method [20] FSIM | Method [3] PSNR | Method [3] FSIM | Method [21] PSNR | Method [21] FSIM | Method [12] PSNR | Method [12] FSIM | Proposed PSNR | Proposed FSIM |
|---|---|---|---|---|---|---|---|---|---|---|---|---|---|
| **CAMERAMAN** | 10 | 34.20 | 0.87 | 33.36 | 0.77 | 34.23 | 0.83 | 34.33 | 0.87 | 34.35 | 0.88 | **34.50** | **0.89** |
| | 30 | 30.80 | 0.79 | 31.00 | 0.77 | **31.40** | **0.80** | 31.05 | 0.75 | 31.22 | 0.77 | 31.20 | 0.77 |
| | 50 | 28.80 | 0.61 | **30.00** | **0.76** | 28.90 | 0.57 | 29.62 | 0.66 | 29.60 | 0.66 | 29.90 | 0.68 |
| **LENA** | 10 | 34.80 | 0.96 | 35.10 | 0.94 | 35.60 | 0.96 | **36.07** | **0.98** | 36.00 | 0.98 | 36.03 | 0.97 |
| | 30 | 31.00 | 0.88 | 31.30 | 0.91 | 30.50 | 0.85 | 31.39 | 0.95 | 31.35 | 0.95 | **31.70** | **0.95** |
| | 50 | 28.50 | 0.72 | 29.30 | 0.84 | 28.10 | 0.68 | 29.07 | 0.92 | 28.96 | 0.92 | **29.15** | **0.93** |
| **PEPPERS** | 10 | 33.30 | 0.95 | 34.30 | 0.92 | 35.00 | 0.97 | 35.03 | 0.95 | 35.01 | 0.95 | **35.10** | **0.97** |
| | 30 | **30.80** | 0.87 | 30.40 | 0.89 | 31.20 | 0.87 | 30.40 | 0.87 | 30.45 | 0.89 | 30.50 | **0.89** |
| | 50 | 28.50 | 0.70 | **29.50** | **0.88** | 28.83 | 0.70 | 29.33 | 0.81 | 29.34 | 0.82 | 29.30 | 0.81 |
| **MANDRILL** | 10 | 32.01 | 0.83 | 32.00 | 0.82 | 32.10 | 0.85 | 32.15 | 0.86 | **32.20** | 0.86 | 32.19 | **0.87** |
| | 30 | 29.50 | 0.75 | 29.45 | 0.74 | 29.78 | 0.75 | 29.85 | 0.76 | 29.95 | 0.76 | **29.96** | **0.76** |
| | 50 | 27.85 | 0.64 | 27.71 | 0.64 | 27.86 | 0.66 | 27.90 | 0.69 | 27.92 | 0.69 | **27.95** | **0.70** |
| **BOATS** | 10 | 34.20 | 0.95 | 35.00 | 0.92 | 35.45 | 0.95 | 35.99 | **0.97** | 35.84 | 0.97 | **36.00** | 0.96 |
| | 30 | 30.56 | 0.87 | 31.00 | 0.90 | 30.35 | 0.83 | 31.35 | 0.94 | 31.21 | 0.93 | **31.50** | **0.95** |
| | 50 | 28.10 | 0.70 | 29.10 | 0.82 | 28.05 | 0.67 | 29.00 | 0.94 | 28.64 | 0.90 | 28.61 | **0.89** |
| **BARBARA** | 10 | 34.63 | 0.94 | 34.93 | 0.92 | 35.57 | 0.93 | 36.00 | 0.96 | 35.93 | 0.96 | **36.00** | **0.96** |
| | 30 | 30.56 | 0.85 | 31.03 | 0.89 | 35.45 | 0.82 | 31.31 | 0.92 | 31.31 | 0.94 | **31.62** | **0.93** |
| | 50 | 28.31 | 0.70 | 29.02 | 0.81 | 27.98 | 0.66 | 29.01 | 0.90 | 28.92 | 0.90 | **29.08** | **0.90** |
| **Bridge** | 10 | 34.75 | 0.95 | 35.09 | 0.94 | 35.61 | 0.96 | 36.06 | 0.98 | 35.99 | 0.97 | 36.02 | 0.97 |
| | 30 | 30.96 | 0.87 | 31.28 | 0.90 | 30.48 | 0.84 | 31.38 | 0.94 | 31.31 | 0.94 | **31.71** | **0.96** |
| | 50 | 28.45 | 0.72 | 29.29 | 0.83 | 28.07 | 0.67 | 29.06 | 0.91 | 28.94 | 0.91 | **29.14** | **0.92** |
| **Parrot** | 10 | 33.31 | 0.94 | 34.28 | 0.91 | 35.04 | 0.98 | 35.01 | 0.94 | 35.00 | 0.95 | **35.09** | **0.98** |
| | 30 | **30.76** | 0.87 | 30.35 | 0.88 | 31.15 | 0.86 | 30.38 | 0.86 | 30.39 | 0.88 | 30.60 | **0.88** |
| | 50 | 28.49 | 0.71 | 29.48 | 0.86 | 28.80 | 0.70 | 29.31 | 0.81 | 29.31 | 0.81 | **29.36** | 0.82 |
| **Cap** | 10 | 34.10 | 0.86 | 33.34 | 0.78 | 34.21 | 0.83 | 34.31 | 0.86 | 34.32 | 0.87 | **34.51** | **0.89** |
| | 30 | 30.74 | 0.78 | 31.02 | 0.76 | **31.38** | **0.81** | 31.00 | 0.73 | 31.20 | 0.76 | 31.22 | 0.79 |
| | 50 | 28.74 | 0.60 | **30.05** | **0.75** | 28.89 | 0.56 | 29.59 | 0.65 | 29.61 | 0.65 | 29.92 | 0.70 |
| **House** | 10 | 34.21 | 0.94 | 35.01 | 0.91 | 35.44 | 0.94 | 35.98 | 0.94 | 35.82 | 0.95 | **36.02** | **0.96** |
| | 30 | 30.45 | 0.86 | 31.01 | 0.89 | 30.33 | 0.82 | 31.30 | 0.91 | 31.20 | 0.91 | **31.49** | **0.94** |
| | 50 | 28.07 | 0.70 | 29.08 | 0.81 | 28.02 | 0.67 | **29.00** | **0.90** | 28.62 | 0.89 | 28.63 | 0.89 |
| **Average** | - | 31.01 | 0.80 | 31.41 | 0.83 | 31.45 | 0.80 | 31.70 | 0.86 | 31.65 | 0.87 | **31.79** | **0.87** |

a) Original Image

b) Noisy Image

c) Method [19]

d) Method [20]

e) Method [3]

f) Method [21]

g) Method [12]

h) Proposed Method

**Fig. 7**. The results of different methods on CAMERAMAN with standard deviation of 10 in dB.

a) Original Image

b) Noisy Image

c) $k = 1$ ,PSNR=30.09

d) $k = 2$ , PSNR=31.8

e) $k = 3$ ,PSNR=31.4

f) $k = 4$ ,PSNR=31.02

g ) Global, PSNR=30.75

h) Proposed, PSNR=33.61

**Fig. 8.** The results of the proposed method with different sparsities and in general on a noisy CAMERAMAN image with a standard deviation of 25.

| **Table IV**. Run time of different methods | |
|---|---|
| **Time(second)** | **Method** |
| 11.21 | Proposed Method |
| 13.85 | Method [20] |
| 38.66 | Method [19] |
| 27.25 | Method [3] |
| 33.56 | Method [21] |
| 11.43 | Method [12] |

## VI. Conclusion

In this paper, a localized AWGN noise reduction method is presented based on SVD basis. In this method, a TI is created using a low frequency component of noisy image and image gradient. The data pertaining to the TI is applied to adaptive optimal low rank appoximation of each patch. The high frequency component of the noisy image will be the input of proposed algorithm. To eliminate the noise of each patch from the high frequency component image, the corresponding patch is extracted from the TI image. If the average of the gradient of the patch exceeds the average gradient of the total TI image, it means that the patch belongs to the textured parts of the image. Therefore, it can be reconstructed using the answer gained from the optimization problem. Conversely, in case the average of the gradient of each patch is not larger than that of total TI image, then the patch belonging to the smooth areas must be reconstructed with less sparsity. This is the set procedure for all the image patches in order to create a high frequency component of denoised image. Combining the high-frequency component of denoised image with the low-frequency component of the noisy image will make the output image. In the proposed method, using adaptive basis for signal representation and ideas like patch labeling and the adaptive determination of the sparsity in the SVD domain has resulted in acceptable speed and computational complexity.

## References


[1] Zhang, X., et al., Compression artifact reduction by overlapped-block transform coefficient estimation with block similarity. IEEE transactions on image processing, 2013. 22(12): p. 4613-4626.

[2] Khan, A., et al., Image de-noising using noise ratio estimation, K-means clustering and non-local means-based estimator. Computers & Electrical Engineering, 2016. 54: p. 370-381.

[3] Takeda, H., S. Farsiu, and P. Milanfar, Kernel regression for image processing and reconstruction. IEEE Transactions on image processing, 2007. 16(2): p. 349-366.

[4] Fan, L., et al., Nonlocal image denoising using edge-based similarity metric and adaptive parameter selection. Science China Information Sciences, 2018. 61(4): p. 049101.

[5] Zhang, X., et al., Gradient-based Wiener filter for image denoising. Computers & Electrical Engineering, 2013. 39(3): p. 934-944.

[6] Shanthi, S.A., C.H. Sulochana, and T. Latha, Image denoising in hybrid wavelet and quincunx diamond filter bank domain based on Gaussian scale mixture model. Computers & Electrical Engineering, 2015. 46: p. 384-393.

[7] Chen, M., et al. An OCT image denoising method based on fractional integral. in Optical Coherence Tomography and Coherence Domain Optical Methods in Biomedicine XXII. 2018. International Society for Optics and Photonics.

[8] shamsi, a., Reconfigurable CT QDSM with mismatch shaping dedicated to multi-mode low-IF receivers. International Journal of Industrial Electronics, Control and Optimization, 2019. 2(3): p. 257-264.

[9] Smirnov, M.W. and D.A. Silverstein, Noise reduction using sequential use of multiple noise models. 2019, Google Patents.

[10] Huang, Z., et al., Progressive dual-domain filter for enhancing and denoising optical remote-sensing images. IEEE Geoscience and Remote Sensing Letters, 2018. 15(5): p. 759-763.

[11] Gavaskar, R.G. and K.N. Chaudhury, Fast adaptive bilateral filtering. IEEE Transactions on Image Processing, 2018. 28(2): p. 779-790.

[12] Guo, Q., et al., An efficient SVD-based method for image denoising. IEEE transactions on Circuits and Systems for Video Technology, 2015. 26(5): p. 868-880.

[13] Aharon, M., M. Elad, and A. Bruckstein, K-SVD: An algorithm for designing overcomplete dictionaries for sparse representation. IEEE Transactions on signal processing, 2006. 54(11): p. 4311-4322.

[14] Elad, M. and M. Aharon, Image denoising via sparse and redundant representations over learned dictionaries. IEEE Transactions on Image processing, 2006. 15(12): p. 3736-3745.

[15] Mallat, S. and G. Yu, Super-resolution with sparse mixing estimators. IEEE transactions on image processing, 2010. 19(11): p. 2889-2900.

[16] Jiang, L., X. Feng, and H. Yin, Structure and texture image inpainting using sparse representations and an iterative curvelet thresholding approach. International Journal of Wavelets, Multiresolution and Information Processing, 2008. 6(05): p. 691-705.

[17] Kalantari, S. and M.J. Abdollahifard, Optimization-based multiple-point geostatistics: A sparse way. Computers & geosciences, 2016. 95: p. 85-98.

[18] Pizurica, A. and W. Philips, Estimating the probability of the presence of a signal of interest in multiresolution single-and multiband image denoising. IEEE Transactions on image processing, 2006. 15(3): p. 654-665.

[19] Zhang, J., et al., Image restoration using joint statistical modeling in a space-transform domain. IEEE Transactions on Circuits and Systems for Video Technology, 2014. 24(6): p. 915-928.

[20] Jiang, J., L. Zhang, and J. Yang, Mixed noise removal by weighted encoding with sparse nonlocal regularization. IEEE transactions on image processing, 2014. 23(6): p. 2651-2662.

[21] Dabov, K., et al., Image denoising by sparse 3-D transform-domain collaborative filtering. IEEE Transactions on image processing, 2007. 16(8): p. 2080-2095.

[22] Dabov, K., et al., Image denoising with shape-adaptive principal component analysis. Department of Signal Processing, Tampere University of Technology, France, 2009.

[23] He, Y., et al., Adaptive denoising by singular value decomposition. IEEE Signal Processing Letters, 2011. 18(4): p. 215-218.

[24] Dong, W., G. Shi, and X. Li, Nonlocal image restoration with bilateral variance estimation: a low-rank approach. IEEE transactions on image processing, 2012. 22(2): p. 700-711.

[25] Mallat, S., A Wavelet Tour of Signal Processing: The Sparse Way (Academic, Burlington, MA). 2008.

[26] Starck, J.-L., E.J. Candès, and D.L. Donoho, The curvelet transform for image denoising. IEEE Transactions on image processing, 2002. 11(6): p. 670-684.
[27] Mallat, S. and G. Peyré, A review of bandlet methods for geometrical image representation. Numerical Algorithms, 2007. 44(3): p. 205-234.
[28] Do, M.N. and M. Vetterli, The contourlet transform: an efficient directional multiresolution image representation. IEEE Transactions on image processing, 2005. 14(12): p. 2091-2106.
[29] Walter, G.G. and X. Shen, Convergence and Summability of Fourier Series, in Wavelets and Other Orthogonal Systems. 2018, CRC Press. p. 93-110.
[30] Eckart, C. and G. Young, The approximation of one matrix by another of lower rank. Psychometrika, 1936. 1(3): p. 211-218.

**Sadegh Kalantari** was born in Tafresh, Iran. He received the B.S. and M.S. degrees in electrical engineering from Tafresh University. He is currently the ph.D student of Control Enginnering in Tafresh University. His current research interests include the areas of system identification, optimization, signal processing, control, quantom computing, geostatistics, and machine learning.

**Mehdi Ramezani** received the Ph.D. degree in applied mathematics and optimal control from Amirkabir University of Technology, Tehran, Iran. He is currently Assistant Professor in Department of Control Engineering, Tafresh University, Tafresh, Iran. His current research interests include the areas of optimal control, system identification, optimization, control, soft computing and machine learning.

**Ali Madadi** received the Ph.D. degree in control engineering from Amirkabir University of Technology, Tehran, Iran. He is currently Associate Professor in Department of Control Engineering, Tafresh University, Tafresh, Iran. His current research interests include the areas of optimal control, robust control, adaptive control, nonlinear control, optimization and system identification.

**IECO**

**This page intentionally left blank.**